Research Square

Preprints are preliminary reports that have not undergone peer review.
They should not be considered conclusive, used to inform clinical practice,
or referenced by the media as validated information.

Megaregional adaptation and recovery priorities preserve local resilience in the US Northeast rail corridor

Auroop Ganguly

a.ganguly@northeastern.edu

Northeastern University https://orcid.org/0000-0002-4292-4856

Jack Watson

Northeastern University

Samrat Chatterjee

Pacific Northwest National Laboratory

Article

Keywords:

Posted Date: March 31st, 2026

DOI: https://doi.org/10.21203/rs.3.rs-8090690/v1

License: This work is licensed under a Creative Commons Attribution 4.0 International License.
Read Full License

Additional Declarations: There is **NO** Competing Interest.

Megaregional adaptation and recovery priorities preserve local resilience in the US Northeast rail corridor

Jack Watson[1,2], Samrat Chatterjee[2,1], Auroop Ganguly[1,3,2*]

[1]Sustainability & Data Sciences Laboratory, Department of Civil & Environmental Engineering, Northeastern University, 360 Huntington Ave, Boston, 02115, MA, USA.
[2]Data Sciences & Machine Intelligence Group, Pacific Northwest National Laboratory, 902 Battelle Blvd, Richland, 99354, WA, USA.
[3]AI for Climate & Sustainability, Institute for Experiential AI, Northeastern University, 360 Huntington Ave, Boston, 02115, MA, USA.

*Corresponding author(s). E-mail(s): a.ganguly@northeastern.edu; watson.jac@northeastern.edu;
Contributing authors: samrat.chatterjee@pnnl.gov;

Abstract

Rail transit systems are vital to urban mobility. This is especially true in emergent 'megaregions' consisting of regional hubs agglomerated into densely interconnected, polycentric conurbations. Infrastructure such as tracks and interchange stations are often shared between urban, regional, and intercity networks, enabling inter-system travel. However, their resilience to hazards is typically assessed on an individual system basis, seeking local optima that risk overlooking global concerns of robustness and adaptive capacity. We introduce a framework for comparative analysis of urban-to-megaregional rail transit resilience, combining measures of connectivity and ridership to capture tradeoffs between local and megaregional adaptation and recovery strategies. Results indicate that megaregional coordination can significantly benefit global resilience while preserving local priorities, with top strategies increasing global resilience by 12-41% and yielding global-local benefit-cost ratios of 2.5-4.3. Furthermore, we find that strictly local assessments poorly capture megaregional priorities, offering minor local benefits while missing opportunities to strengthen megaregion-wide resilience.

1 Main

Rail transit networks (RTNs) are essential for sustained economic activity within urban agglomerations, while being increasingly exposed to the impacts of natural and manmade hazards. The Northeast Corridor (NEC) of the United States is the largest megaregion in the world by GDP, generating approximately $5.8 trillion USD within 2% of national land area [1]. The NEC is polycentric, with hub cities including New York, Washington, Philadelphia, Boston, and Baltimore. The NEC's RTNs consist of urban rapid transit systems (URTS), regional commuter rail (RCR), and intercity passenger rail (IPR). These systems are interconnected, interdependent, and often share common-benefit infrastructure such as stations and tracks, designed for efficient passenger interchange. However, decision-analytic frameworks for resilience-enhancing investments in RTNs and strategies for post-disaster recovery triage typically limit their analysis to a particular system or scale, rather than the megaregional, multi-scale network-of-networks (NoN) they comprise [2–4]. Impacts to RTNs are correlated due to concentration in regional hubs. For example, in 2011, Hurricane Sandy inflicted more than $4.5 billion in damage to RTNs in Greater New York [5], severing the NEC's north and south components by flooding tunnels under the Hudson River, and disrupting at least seven RTNs [6].

Through topological analysis of fifteen of the NEC's RTNs, we demonstrate how asset-level priorities for adaptation and recovery diverge when considering a system in an isolated 'local' context versus a connected 'global' one, finding that megaregional prioritization effectively reflects local priorities, while local prioritization poorly captures megaregional ones. These results suggest that planners risk overlooking assets important to megaregional robustness and recovery by over-constraining system boundaries. This study considers the prioritization of transit stations using connectivity and ridership, but presents a framework for comparative analysis of multiscale infrastructure networks that generalizes to other asset-level importance measures and infrastructure types. These findings highlight the need for novel policy frameworks for resilient decision-making that cut across system boundaries and jurisdictions.

Recent studies have considered multiple RTNs as an interconnected NoN. Most have limited their scope to several urban and regional systems within single metropolitan areas (e.g., [2, 4, 7–9]). Those with wider geographic scope have focused on intercity rail while excluding urban and regional systems from their analyses (e.g. [10–13]). Findings from studies of multi-modal transit systems suggest that inter-modal transfer nodes contribute significantly to the overall robustness of a NoN [2], and that failure to consider passenger flow between systems can bias estimates of resilience by excluding routes through interchanges [8].

We define two scales of analysis to compare local strategy (S-L) and global strategy (S-G). S-L assesses individual urban, regional, and intercity systems excluding connections to other RTNs. S-G considers a system connected to others through interchange stations. We conduct a series of experiments to measure the relative resilience contributions of each RTN's stations locally and globally, using five node-level metrics that incorporate centrality, efficiency, and ridership. The resilience of the NEC and its RTNs is measured and cost-benefit analysis performed to reveal resilience tradeoffs.

Results show that, across metrics, S-G yields marginal shifts in the rankings of locally-prioritized stations in the majority of RTNs. This indicates that local resilience can be preserved in megaregional planning. However, S-L poorly captures global priorities, missing opportunities to strengthen megaregional resilience. This trend is most pronounced in RTNs central to the NEC, such as the NYC Subway, and weakest in its peripheries.

Our findings indicate that the most effective prioritization strategy varies by scale, position, and disruption stage. On average, the most effective metric for each system under S-G improved megaregional recovery performance by 14.9% relative to S-L across URTS, 22.0% across RCR, and 12.0% for IPR. In failure simulations, S-G was more effective than S-L by 141.0% for URTS, 101.8% for RCR, and 23.2% for IPR.

2 Results

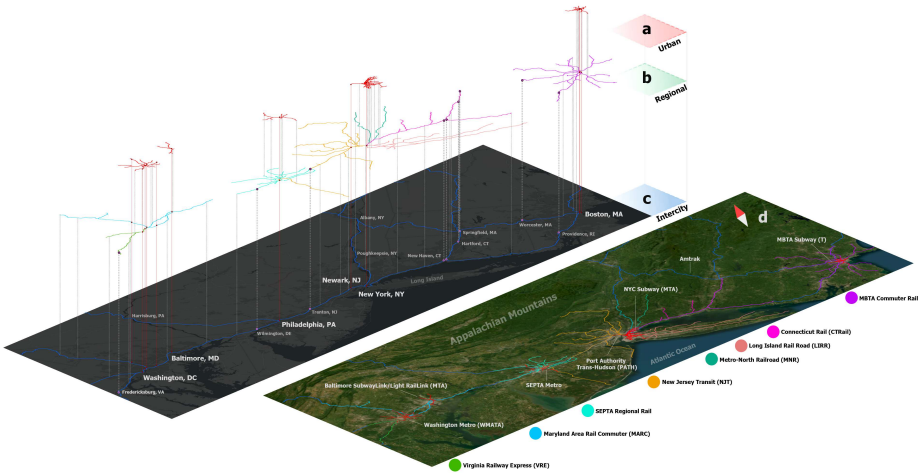


Fig. 1 RTNs of the Northeast Corridor. **a.** urban rapid transit (red), including the MBTA subway (Boston), New York City Subway, PATH (New York/New Jersey), SEPTA Metro (Philadelphia), Baltimore SubwayLink & Light RailLink, and Washington Metro. **b.** regional commuter rail, colored by system, including the MBTA commuter rail (Eastern New England), CT Rail (Connecticut), Metro-North Railroad (New York, North and East), Long Island Rail Road (New York/Long Island), NJ Transit (New Jersey), SEPTA Regional (Southeast Pennsylvania), MARC (Maryland/Washington), and VRE (Northern Virginia/Washington). **c.** long-distance intercity passenger rail (dark blue), operated by Amtrak. **d.** the Northeast Corridor megaregion, the most densely populated megaregion in the US and the highest-GDP megaregion globally. **Connections:** dashed gray lines denote interchange stations connecting urban and regional or regional and intercity systems. Bolded lines show regional hubs. Solid red lines indicate interchanges that connect all three scales of RTN within a single station.

The NEC is comprised of 15 urban, regional, and intercity passenger rail systems (Figure 1). These include 6 URTS (Fig. 1.a) serving Boston, New York City, Newark, Jersey City, Philadelphia, Baltimore, and Washington, D.C.; 8 RCR (Fig. 1.b), and

national IPR (Fig. 1.c). A full list of this case study's RTNs and associated descriptive statistics are presented in Table 1.

2.1 Local peripheries act as megaregional bridges

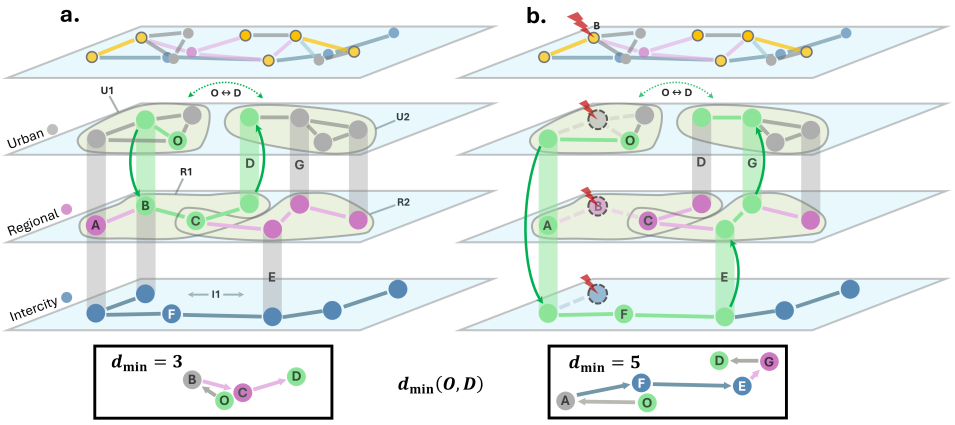


Fig. 2 Passengers travel through RTNs beginning at an origin O and arriving at a destination D. Three vertical layers show the urban, regional, and intercity RTNs present within a megaregion; the topmost layer shows a superposition of these systems as a network-of-networks. Vertical columns correspond to interchange stations present in multiple transit layers, at which passengers can navigate between separate RTNs to reach their destinations. Shortest paths from $O \rightarrow D$ are highlighted green, with arrows showing interchanges taken within those paths. Scenario **a.** shows the shortest path between an origin and destination in two URTS (U1, U2) in neighboring regional capitals during normal operating conditions. A passenger begins in U1, interchanges to RCR R1 at B, and continues to destination D. In **b.**, a disruption renders B impassable, and the shortest alternate route is highlighted: our passenger interchanges from U1 to IPR I1 at station A, rides IPR to R2 via interchange E, and again interchanges to their destination in U2 via G. Stations that are of secondary importance when considering individual systems in isolation, such as relatively peripheral A, are revealed to be critically important when inter-system travel is considered. Moreover, disruptions in one RTN can induce shifts in traffic patterns in other RTNs, revealing alternate pathways critical to megaregional robustness during adverse conditions.

The individual RTNs composing the NEC are highly coupled, sharing interchanges, right-of-way corridors, and track segments [14]. Travel between cities and regions can require navigating multiple systems through interchanges. The scenarios presented in Figure 2 were chosen to demonstrate how the resilience of megaregional rail depends on this inter-system connectivity structure. Stations (A, B) are of minor importance in a single-network view. When B is disrupted, all other stations in U1 remain mutually reachable (Fig. 2.b). Secondary failure in R1 is limited to a single station's disconnection, and as an intercity terminus, all other routes in I1 are unaffected. Globally, however, B is a central node critical to inter-system traffic flow. Likewise, A is peripheral within each RTN, but is an important interchange between them. This is especially true during disruptions; A is the only node connecting U1 to other RTNs when B fails. This underscores the role of interchange redundancies in megaregional robustness, and

the cascading impacts that disruptions to one RTN can have on others, even without direct connections.

URTS and RCR tend to exhibit core-periphery structure. This is in contrast to the NEC's IPR, which resembles a mesh with uniform degree distribution and weak community structure. The placement of interchanges connecting RTNs exhibits a bimodal pattern: interchanges are typically either central hubs in urban cores, such as Manhattan's Penn Station and Boston's Back Bay, or are situated peripherally near line termini to facilitate commutes from suburban and exurban locales, and to allow for long-distance transfers between IPR and more frequent RCR and URTS [15].

Somewhat counterintuitively, this leads to the set of the most megaregionally important stations being largely comprised of the most and least locally important stations. The former are inner-city 'hub' interchanges: Back Bay, NY Penn Station, and Washington Union are highly central to local URTS and RCR while creating pathways between them. The latter are stations locally peripheral, such as Worcester, Forest Hills, and Braintree stations (MBTA), Norristown and Fern Rock (SEPTA), and New Carrollton, Rockville, and Greenbelt (WMATA, MARC). Viewed from a single-system perspective, these stations are superfluous to the structural resilience of one or more RTNs; of eight examples, seven are an urban or regional terminus, otherwise preserving intra-system navigability upon disruption. The exception is New York, wherein almost all interchanges between the URTS, RCR, and IPR are hubs.

2.2 Local and global prioritization strategies

To assess the degree of alignment between local and global priority rankings, the centrality of each RTN's stations was measured locally in isolation, and globally with interchanges connected the the surrounding networks. First, the top-10 priority stations were locally determined (R_L). To assess the degree to which global rankings reflect local priorities, the globally determined rank (R_G) of the same stations was subtracted from corresponding S-L to obtain $\delta R_{L\to G}$, and vice versa ($\delta R_{G\to L}$, Fig. 3.b).

Large negative values of $\delta R_{L\to G}$ (RGB) indicate that locally high-priority stations are not well-reflected globally; highly negative $\delta R_{G\to L}$ indicate that megaregional priorities aren't well-reflected by S-L. Across scales and systems, S-L fails to capture S-G, while S-G preserves S-L more consistently. This is reflected in an average top-10 $\delta R_{G\to L}$ of -29.97% and an average $\delta R_{L\to G}$ of -8.00% (Fig. 3.a).

At a high level, this phenomenon can be explained in information theoretic terms: S-G captures S-L more effectively than S-L captures S-G because local information is included in global analysis, while S-L by definition excludes information about other systems. A graph contains the set of all possible induced subgraphs, while each subgraph contains only a fraction of information about the graph it was induced from. S-G is then in theory capable of balancing local and global resilience priorities, while S-L will always prioritize purely local resilience.

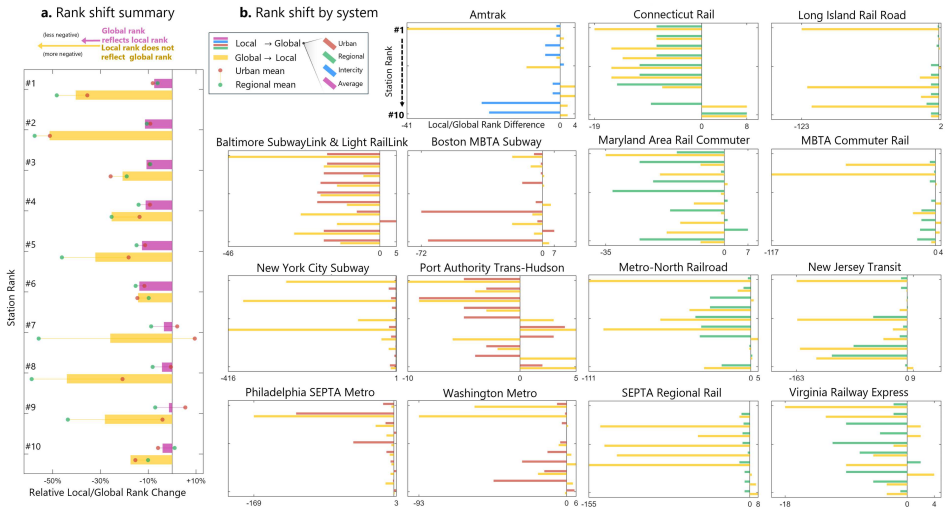


Fig. 3 Histograms show the relative change in the ridership-weighted betweenness centrality (RWBC) ranking of an RTN's top 10 stations measured locally and globally. Gold bars show global-to-local rank shifts, while red, green, blue, and purple bars show local-to-global rank shifts (rank shift when globally top-ranked stations are measured locally). Negative values indicate a drop in rank; the larger the magnitude, the greater the drop in ranking. Gold bars more negative than corresponding RGB indicate global strategy reflects local priorities more than local strategy reflects global priorities, and vice versa. Positive or weakly negative values indicate a sharing of local and global priorities. **a.** shows average rank shifts for each RTN's top-10 stations, with overlays disaggregating urban and regional scales. **b.** shows rank changes corresponding to each of the NEC's fifteen individual RTNs.

2.3 The influence of interchange placement and intermodal pathways

To illustrate the rank-shift process, Figure 4 provides detail on one URTS, RCR, and IPR, using metropolitan Boston's MBTA Subway and Commuter Rail as respective urban and regional case studies.

On an urban scale, stations that are relatively peripheral increase in ranking locally to globally, while hubs decrease in rank. This pattern is explained by interchange placement away from the urban core. Regionally, the MBTA Commuter Rail consists of two Northern and Southern connected components, their respective hubs being North and South Station. (A 'North-South Rail Link' connecting the two via tunnel has been a subject of proposals since at least 1987 [16]). The two hemispheres of the network are connected only via interchange through URTS, yielding a large discrepancy between R_L and R_G. RCR exhibits an inverted pattern compared to URTS: stations in the core exhibit higher R_G than R_L as North and South Stations act as bottlenecks connecting regional components via URTS. Meanwhile, alternate routes through the subway's peripheral interchanges de-prioritize stations that serve as choke points connecting RCR to the core.

Amtrak IPR sees the least-pronounced δR and inconsistent spatial-connectivity patterns. One explanation is that IPR connectivity and ridership partially reflects that

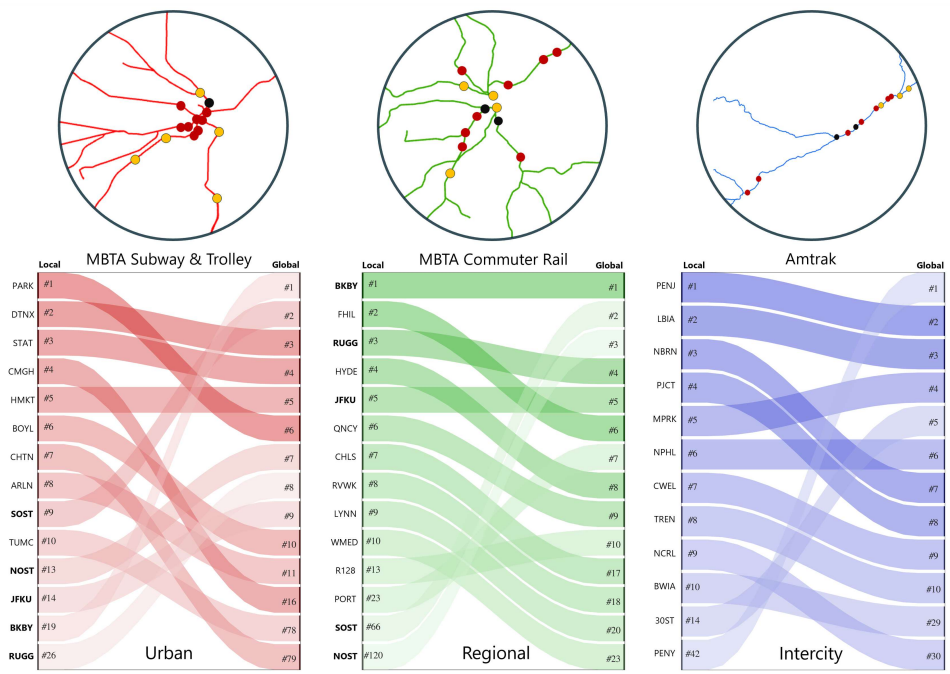


Fig. 4 Bottom: Station rankings measured by RWBC, for the MBTA Subway, MBTA Commuter Rail, and Amtrak IPR. The left side of each panel shows local priority ranks R_L, the right-hand side global ranks R_G, and connections indicate rank-shifts δR. **Top:** station locations within the corresponding networks. Stations in red indicate higher local than global ranking ($\delta R_{G\to L} > 0$); stations in gold, higher global than local ($\delta R_{L\to G} > 0$). Stations in black indicate no rank change ($\delta R_{G\to L} = \delta R_{L\to G} = 0$). Station names are displayed as four-character abbreviations, with bolded text indicating interchanges present in both urban and regional rankings.

of the NEC, as urban interchanges exhibit high intercity ridership and are centrally located, and most inter-module bottlenecks are IPR assets.

2.4 Failure and recovery simulations

To test the effects of strategy on local (R-L) and global (R-G) resilience, sequential failure and recovery were simulated. Failure (node removal) models a simplified process of vulnerability assessment informing investment in protective measures (e.g., flood-proofing, retrofitting). Stations for which disruption results in greater impacts may be prioritized; others will necessarily be passed over under limited resources. Recovery (node reactivation) reflects post-disaster response. Dispatching recovery resources (e.g., repair crews) entails a triage process prioritizing the restoration of certain assets before others. Network efficiency was calculated after each alteration to reflect the ability of traffic to flow throughout a system.

For each RTN a total of four curves were produced for each importance measure (Fig. 5.b). Instantaneous performance is denoted as $\rho(x)$, with $x = (G_C, G_I, S_C, S_I)$ correspond to combinations S-G/R-G, S-L/R-G, S-G/R-L, and S-L/R-L, respectively.

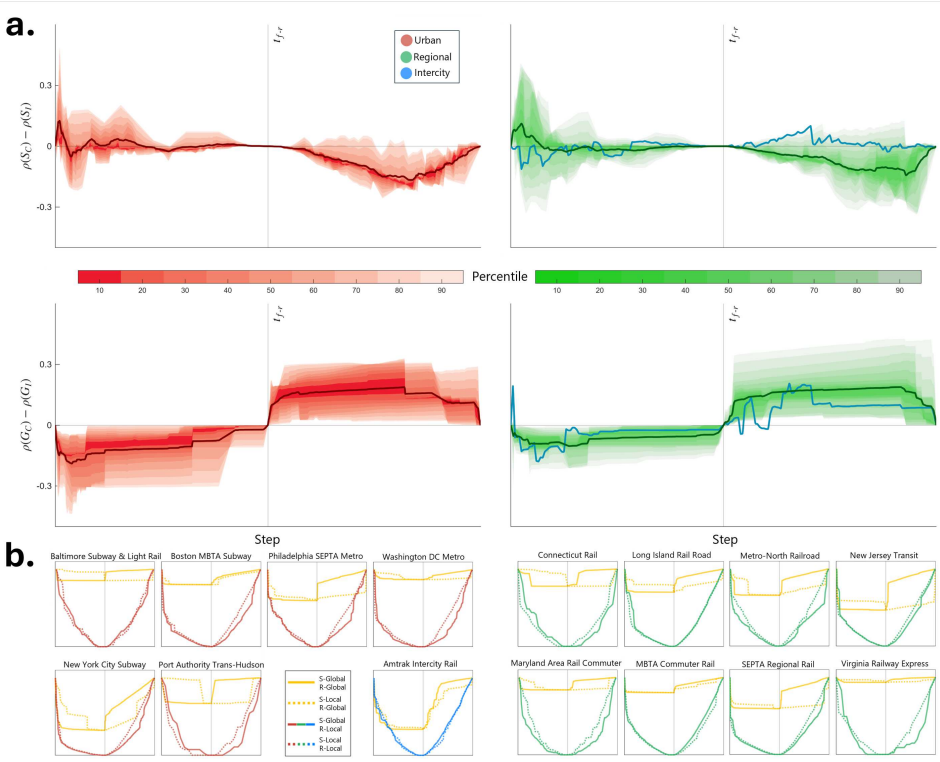


Fig. 5 Resilience curves show failure and recovery when stations are deactivated and reactivated sequentially. Using RWBC to determine removal and addition sequence, **b.** shows gold lines corresponding to megaregional (R-Global) system performance, with RGB lines corresponding to urban, regional, and intercity system performance (R-Local). Solid lines indicate removal and addition sequence determined by megaregional strategy (S-Global), with dashed lines corresponding to S-Local. **a.** shows the difference in performance between S-L and S-G for particular systems (top) and the NEC (bottom). Average values are provided disaggregated by scale, with confidence intervals showing 5th-95th percentiles for urban and regional systems, and the single IPR on the same axes as RCR. Without exception, global prioritization is more efficacious for megaregional failure and recovery, while local failure and recovery shows a greater deal of heterogeneity.

The expected patterns of resilience in the recovery phase are (1) S-G leading to higher R-G than S-L, and (2) S-L leading to higher R-L than S-G. For failure the null hypothesis is reversed, with global (local) prioritization expected to degrade global (local) performance more effectively than local (global) strategy. This assumption holds for R-G in all 15 RTNs: S-G is more effective than S-L at degrading and recovering the NoN. The difference in R-G outcomes between S-L and S-G is most pronounced in RTNs important to megaregional connectivity, specifically those within the NEC's 'central module' (NY-NJ-PA). R-G is least sensitive to strategy for RTNs in Northern and Southern modules (New England and MD-DC-VA). Furthermore, RTNs within these peripheral modules exhibit greater sensitivity to strategy choice, making prioritization that puts greater weight on local considerations more favorable in terms of

R-G/R-L tradeoffs. S-G consistently results in higher R-G across metrics and phases (Fig. 5.a). R-L is less consistent, with S-L on average more effective across phases, but varying significantly between RTNs. For IPR, across phases, both local and global resilience mutually benefit from global strategy. This reinforces the notion that IPR functions as a proxy for the NEC-at-large.

2.5 Resilience tradeoffs in local and global prioritization strategies

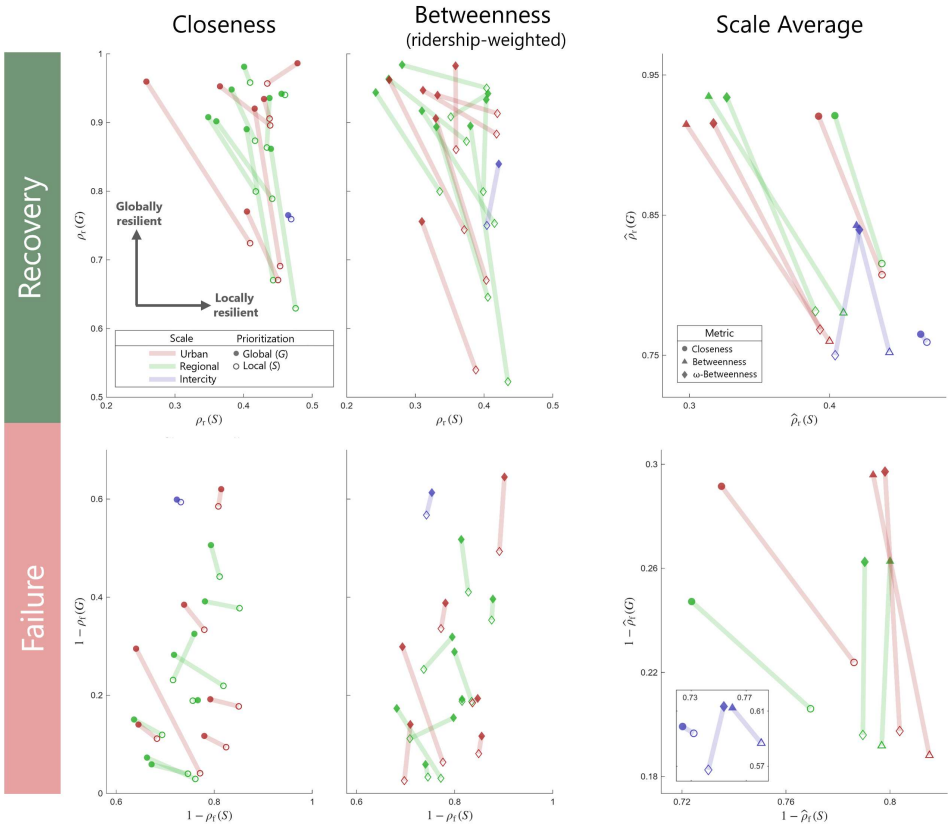


Fig. 6 Local (R-L, $\rho(S)$) and global resilience (R-G, $\rho(G)$) outcomes for two of the most effective prioritization strategies, closeness centrality and ridership-weighted betweenness centrality. **Top:** local and global resilience during the recovery phase $\rho_{\mathrm{r}}(S)$ and $\rho_{\mathrm{r}}(G)$ for CC and RWBC. S-G/CC preserves R-L more effectively than RWBC, while in absolute terms, RWBC results in greater regional and intercity resilience. **Bottom:** targeted failure serves as a proxy for adaptation prioritization. RWBC proves superior to CC and unweighted BC in both relative and absolute terms. S-G/RWBC is more effective at degrading system performance both globally *and* locally relative to S-L/RWBC.

Performance was integrated with respect to time both phases and normalized to capture resilience in a single value. For each combination of RTN, importance measure,

and prioritization strategy, total R-L and R-G were plotted on opposing axes (Fig. 6). The two points corresponding to outcomes of S-L and S-G were connected to highlight relative changes in R-L and R-G as a function of strategy. The slope of the connecting line represents the change in R-G with respect to R-L when switching from S-L to S-G. Consistent across all importance metrics, RTN scales, and simulation phases, global resilience sees greater benefits than the accompanying cost to local resilience when switching from local to global prioritization strategy.

In the recovery phase, CC was by a wide margin the most effective metric at mitigating negative impacts to R-L when switching to S-G for urban and regional systems, with average global-local BCR of 2.50, 3.15, and 1.30 for urban, regional, and intercity RTNs, with corresponding gains in global resilience of 14.0%, 12.95%, and 0.75%. Closeness also resulted in the highest R-G for URTS by a slim margin. Under S-L, closeness outperformed all other metrics in maximizing R-L for all three RTN scales. Furthermore, S-L/CC resulted in the highest R-G of all metrics. In a scenario in which regional or megaregional coordination is not possible due to policy barriers, these results suggest that CC can be used as a recovery prioritization heuristic to effectively restore system performance of both individual RTNs and the NEC as a whole.

Under S-G, the highest R-G resulted from RWBC for URTS and (unweighted) BC for RCR and IPR. However, the difference in R-G values between RWBC and BC was negligible, while RWBC offered other benefits: foremost, a mitigated decrease in R-L, with RWBC increasing the global-local BCR of BC from 1.51 to 1.94. RWBC gave a desirable combination of the benefits of BC and CC: high absolute R-G with R-L greater than BC but less than CC. Depending on stakeholder priorities, CC and RWBC emerge as the two most favorable metrics for recovery.

The ability of a system to absorb the impacts of a disruption is referred to as the robustness of the system; this is a compact synonym for descriptions such as *failure phase resilience*. The performance of each metric was evaluated as the ability to effectively degrade a network. Accordingly, lower values of robustness ρ_f indicate a more effective strategy, and values of $1 - \rho_f$ were plotted (Fig. 6) to allow direct comparison with recovery.

Under S-G, DC, RWBC, BC, δE, and CC resulted in marginally different R-G, with DC yielding the greatest for URTS and IPR and δE for RCR. In contrast to recovery, closeness gave the lowest R-G and R-L across both S-L and S-G and all three RTN scales. S-G/DC resulted in superior R-G while yielding the highest R-L of any metric across scales, giving urban, regional, and intercity BCRs of 3.41, 4.31, and 2.73, with only marginal R-L loss in exchange for considerable average R-G gains of 23.2-41.3%.

In failure simulations, treated as a proxy for adaptation planning, S-G saw global-local BCRs of 6.00, 2.60, and 1.91 for urban, regional, and intercity RTNs, respectively, averaged across all metrics. The corresponding recovery phase BCRs were 4.56, 2.20, and 2.27. These statistics omit cases in which S-G was mutually beneficial to R-G and R-L. For recovery, these scenarios include DC-regional, DC-intercity, and RWBC-intercity, and for failure, δE-regional, BC-regional, RWBC-regional, and RWBC-intercity. Overall, these results suggest that megaregionally-coordinated resilience planning may have BCRs that increase megaregion-wide resilience by

200-600% relative to local opportunity costs. For RCR and IPR, results show that coordination on a broader scale can directly benefit local RTN resilience.

3 Discussion

Across five importance metrics, transitioning from S-L to S-G resulted in favorable resilience outcomes in a majority of cases. Megaregional resilience saw significant gains with comparatively small tradeoffs to R-L. While optimal prioritization metrics vary between systems and depend on stakeholder priorities, R-L was largely maintained in megaregional strategies, and in some instances, S-G was mutually beneficial to both R-L and R-G for regional and intercity rail.

The utility of this study is in its potential to inform the megaregional coordination of infrastructure resilience planning. Roughly 70-80% of capital infrastructure projects in the U.S. are financed via the $4 trillion municipal bond market [17, 18]. Yet, coordination can become increasingly complex as projects cross multiple jurisdictions. Regional transit and flood protection systems, for example, often involve distinct bond issuers, who may have varying fiscal strength, legal authority, and repayment capacity. Consequently, it may often be unclear how to apportion both the cost burden and risks associated with participating issuers fairly. Academic literature on cost-sharing in regional infrastructure supports the notion that a lack of a consistent framework for allocation can slow or complicate investments [19].

Credit ratings play a critical role in municipal bond issuance, wherein issuers with higher ratings generally benefit from lower borrowing costs, as the market perceives them as a lower credit risk and likely strong repayment capacity[20]. When projects span multiple jurisdictions, issuing entities can often vary in their ratings [21]. In the U.S., many transit agencies issue revenue bonds, a type of municipal bond. These are secured by fares, tolls, subsidies, or tax revenue. In some jurisdictions these bonds are issued directly by the agency, while in others they may be issued by a governmental entity on their behalf. Eight of the nine system operators in this study, for example, issue revenue bonds.

Quantifying the benefits and opportunity costs to each issuer for particular adaptation measures can provide empirical guidance for cost sharing frameworks for megaregional investments in infrastructure resilience. Approaching the challenge from another angle and beginning with each agency's budget constraints, such a framework can plausibly enable the identification of particular investments that align with predetermined capital project budgets among stakeholders, benefiting each proportionally to relative contributions.

Certain local benefits of megaregional resilience are not captured in this study. For example, S-L intentionally excludes interchange passenger flow recorded as part of other systems. However, due to inter-system flow not captured in reported statistics, it's likely that a portion of each station's ridership results from interchange, the revenue of which would be impacted by megaregional disruptions. Additionally, further studies of potential local economic benefits from strengthened megaregional resilience could incentivize wider cooperation. The literature on interchange stations has predominantly focused on their role in route choice, travel time, and efficient pedestrian

interchange (e.g., [22, 23]). Research must be done on their influence on the systems they connect, in terms of performance, demand, and economic benefit.

The heuristics employed herein rely on network topology and ridership, making several simplifying assumptions. Passenger flow was synthetically generated; it is not empirical. This was due to a lack of publicly available observational data. Extending analysis with empirical data, such as that inferred from Origin-Destination-Transfer models [24], could improve accuracy and reduce uncertainty. Second, network efficiency is used to measure performance for resilience quantification. While efficiency captures the structural impacts of disruptions, it inadequately captures resilience in terms of service performance [9]. Lastly, rail segment geometry is simplified, with edge weights determined as geographic distances between stations. Incorporating realistic measurements of track length and travel time can improve outcome accuracy.

In this study, failure and recovery simulations are limited to sequential removal and addition; time is implicit. Real natural hazards induce multi-faceted impacts and often take the form of compound extremes, with complex temporal and spatial evolutions and damage from intersecting factors such as coastal and pluvial flooding, wildfire, and windstorms. Vulnerability is influenced by indirect failure from damage to other infrastructures, preexisting protective measures, human behavior, and emergency management. Experiments combining simulated exposure to local or regional hazards with models of asset-level vulnerability (e.g., [25]) are necessary for rigorous megaregional resilience planning.

Comprehensive vulnerability assessments for RTNs must include consideration of other infrastructure systems on which rail systems depend. This includes electrical grids and traction networks supplying electrified rail lines, telecommunications for signaling and emergency response, and during floods, urban drainage systems [26–29]. In addition to sewers, the accuracy of flood resilience assessments for RTNs operating tunnels (e.g., urban metros) depends on model representation of inflow locations through which surface runoff can infiltrate, such as station entrances and tunnel portals [30].

This work employs centrality measures as proxies for station-level contributions to system-level robustness and recovery. While metrics such as BC have been shown to serve as effective heuristics, a more comprehensive understanding can be provided by comparing such approximations to optimal or near-optimal solutions. However, the time complexity of combinatorial optimization required to arrive at optimal solutions can be prohibitive for very large networks. While heuristics such as genetic algorithms and simulated annealing can at least partially overcome such limitations [9, 31], achieving convergence on megaregional scales remains a challenge. Recent approaches to similar problems using deep reinforcement learning may be promising in addressing these issues.

In addition to the areas identified specific to multiscale rail systems, this framework has potential applications in the combined analysis of qualitatively different systems such as power, water, mutlimodal transportation, and telecommunications networks. For example, undergrounding power lines is a common resilience-enhancing measure in electrical transmission and distribution systems [32]. The optimal solution with a grid resilience-maximizing objective may differ from the solution that maximizes the combined resilience of power, rail transit, and water distribution systems; applying a

similar framework to such cases would enable quantifying resilience tradeoffs between multiple systems overlapping spatially within the same locality, as opposed to this study, which focuses on multiple qualitatively similar systems of different scales across a large geographic area. This would likewise further the goal of quantifying relative benefits to stakeholders for cost allocation agreements in large capital projects.

4 Methods

4.1 Study area and data

The case study selected for this investigation is the Northeast Corridor of the United States, covering the Atlantic coastal regions from New England in the North to greater Washington, D.C. in the South. Major cities include Boston (Massachusetts), New York (New York), Newark and Jersey City (New Jersey), Philadelphia (Pennsylvania), Baltimore (Maryland), and Washington, District of Columbia, all of which are served by URTS and RCR. The RTNs in this study consist of $1,659$ stations and $1,822$ rail segments in an undirected graph. 91 stations (5.5%) are interchanges bridging multiple systems, 12 of which connect URTS, RCR, and IPR within a single station. The NEC is modeled as a connected graph, with all stations mutually reachable under normal conditions. If IPR is excluded, URTS and RCR form three connected components corresponding to the megaregion's densest regional hubs: Eastern New England in the North, New York-New Jersey-Philadelphia in the Mid-Atlantic, and Baltimore-Washington to the South. (The term *Northeast Corridor* is also commonly used to refer to the specific intercity rail line running between Boston and Washington, D.C.; for clarity, all uses refer to the collective RTNs within the Northeast Megaregion as a whole.)

Station location and connectivity was assembled from public system maps and geospatial layers published by transit agencies. An L-space representation was selected to reflect a focus on structural resilience [33]. Interchanges were consolidated into single nodes to reflect realistic topology and network statistics, rather than being modeled as multiple neighboring nodes in close proximity. This preserves the network's degree distribution and avoids positively biasing resilience by introducing artificial redundancies. In New York City, many nominally-separate stations are constituents of larger subterranean station complexes that serve multiple lines, with separate gates for each station in a complex. Complexes were treated with the same approach as interchanges, condensed into single nodes. Descriptive statistics for each network are presented in Table 1.

Station-level ridership was incorporated into betweenness centrality as ridership-weighted betweenness centrality (RWBC). Ridership was defined as total annual unlinked trips for fiscal year 2019 to provide a stable (pre-COVID-19) baseline. In instances where FY2019 ridership was unavailable, but data for other intervals was, values were adjusted using the ratio of total system ridership for FY2019 to that of the available period. In a minority of cases in which data was not publicly available from the agencies themselves, secondary sources were employed, such as Open Public Records Act request results subsequently shared in public repositories. A detailed description of data sources is provided in the supplement. Interchanges possess unique

Table 1 Rail transit network summary statistics

System	Scale	Nodes	Edges	Cycles	Avg. Degree	Avg. Shortest Path (km)
Amtrak	Intercity	100	100	4	2	20.63
MBTA Subway	Urban	126	128	6	2.032	14.57
NYC Subway	Urban	423	472	$> 10^4$	2.231	21.36
PATH	Urban	13	14	2	2.154	3.58
SEPTA Metro	Urban	172	176	19	2.047	24.86
Baltimore SL/LRL	Urban	47	45	0	1.915	10.01
Washington Metro	Urban	97	101	7	2.083	12.64
MBTA Commuter Rail	Regional	140	140	2	2	12.34
CT Rail	Regional	22	21	0	1.910	6.93
Metro-North Railroad	Regional	114	113	0	1.983	27.12
Long Island Rail Road	Regional	125	127	6	2.032	15.54
NJ Transit	Regional	167	177	146	2.120	19.88
SEPTA Regional Rail	Regional	162	162	1	2	17.82
MARC	Regional	42	42	1	2	11.18
VRE	Regional	19	18	0	1.895	6.29

Table 2 Descriptive statistics for the NEC's 15 RTNs. *Nodes* and *Edges* give the count of passenger stations and track segments. *Cycles* is the count of unique circular paths in each network; RTNs with no redundant connections, resembling branched spanning trees, have none. The NYC Subway, with a high edge density connecting 423 nodes, possesses a cycle count large enough to be computationally prohibitive. *Avg. Degree* is the mean count of connections each station has to neighbors. RTNs with a high edge density, such as the NYC Subway and NJ Transit, have high average degrees. *Avg. Shortest Path* gives the mean path length over $N(N-1)$ unique station pairs.

ridership values for each RTN served. For S-G, ridership was calculated by summing values for each RTN. For S-L, weighting incorporated only that of the particular RTN.

4.2 System representation

In the RTN graph $G = (V, E)$, edges in set E represent the track segments connecting stations. Edge $(i, j) \in E$ connecting stations i and j has a weight w_{ij}, representing traversal cost.

In L-space RTN representations, w_{ij} typically reflect one or more attributes: the path length of the rail segment [34, 35], the time duration required to traverse it [33, 36], or proxies of passenger flow such as average demand [37, 38] or trains per unit-time [10]. Some leave edges unweighted for a strictly topological analysis [39, 40], while others propose composite metrics integrating several features [41, 42]. For example, w_{ij} could be treated as the averaged time difference between arrivals at stations i and j given an operator's published schedule or empirical arrival and departure data. This study weights edges with distance. There are generally two approaches to measuring distance: the first is to measure distance as the path-dependent physical length of the segment. The second is a simplified approach that measures the geodetic distance between nodes, disregarding the physical path of rail segment (i, j) [43–45].

This study takes the second approach, calculating w_{ij} as the Haversine distance between i and j on a spherical Earth with a radius of $r = 6371.0088$km. Letting λ_i, ϕ_i be the longitude and latitude of station i, the differences between stations (i, j) is defined as $\Delta\lambda_{ij} = \lambda_j - \lambda_i$ and $\Delta\phi_{ij} = \phi_j - \phi_i$. The points' central angle is $\theta_{ij} = \frac{d_{ij}}{r}$, where d_{ij} is the spherical distance. Solving the Haversine function for d_{ij} gives the formula used to derive edge weights (Equation 1). Distances are then rescaled prior to weighting.

$$w_{ij} = d_{ij}^{\text{hav}} = 2r \arcsin\left(\sqrt{\frac{1 - \cos\Delta\phi_{ij} + \cos\phi_i \cos\phi_j (1 - \cos(\Delta\lambda_{ij}))}{2}}\right) \tag{1}$$

While computing edge weights as Haversine distances sacrifices accuracy for parsimony, it provides a suitable approximation of segment distance, as maximizing operational efficiency and capital expenditure when planning rail systems dictates constructing the shortest possible path between adjacent stations, with deviation from the shortest path determined by physical constraints such as obstacles in the built and natural environment. Previous work conducting sensitivity analysis suggests that this simplifying assumption is reasonable and does not unduly bias results [44].

4.3 Ridership demand simulation

Calculating RWBC requires weighting each origin-destination (OD) pair with normalized passenger flow volume traveling between them. A doubly-constrained (entropy-maximizing) gravity model with an inverse power law deterrence function was applied to generate an OD matrix for all stations. Model choice was informed by empirical evidence supporting its suitability for both URTS [46] and interurban, megaregional IPR, supported by human mobility data from within Northern China's Beijing-Tianjin-Hebei megaregion [47]. In a gravity model, an iterative process converges on values of $a_i \geq 0$ and $b_j \geq 0$, factors balancing row and column sums of traffic flow. Flow from i to j is expressed as $T_{ij} = a_i b_j P_i A_j f(d_{ij})$, where P_i is trip production, A_j is arrivals, and $f(d_{ij})$ is the deterrence function defining the relationship between path distance and attraction strength.

An inverse power law was selected as the form of the deterrence function to enable traffic flow between distant regions. This was chosen over an exponential function which, in contrast, would cause attraction strength to decay exponentially with distance, risking the overestimation of traffic in URTS and underestimation in RCR and IPR. Comparative analysis of several deterrence functions applied to China's national railways support the notion of the power law as the most suitable choice compared to other functional forms [48]. This deterrence function takes the form

$$f(d_{ij}) = \begin{cases} d_{ij}^{-\alpha}, & i \neq j, d_{ij} < \infty, \\ 0, & i = j \text{ or } d_{ij} = \infty. \end{cases} \tag{2}$$

where d_{ij} is the weighted network distance between i and j, and $-\alpha$ is the power law exponent. In matrix form deterrence is expressed as $F = [f(d_{ij})]_{i,j} \in \mathbb{R}_+^{n \times n}$. Equation

3 describes the row and column constraints that must be satisfied. This is rearranged to solve for factors (a_i, b_j), estimated through an iterative process. This process halts when row and column sum errors fall below a suitably small maximum threshold ϵ_g (Equation 4).

$$\sum_{j=1}^{n} T_{ij} = P_i, \qquad \sum_{i=1}^{n} T_{ij} = A_j \tag{3}$$

$$\epsilon_g \leq \max \left\{ \max_i \left| \sum_j T_{ij} - P_i \right|, \max_j \left| \sum_i T_{ij} - A_j \right| \right\} \tag{4}$$

A power law exponent of $\alpha = 3/2$ was chosen as a reasonable default value for the deterrence function in lieu of the observational data needed for empirical parameter estimation. Studies report empirical estimates of α in range $1 \leq \alpha \leq 2$ for passenger rail systems, informing the value used in this study [46, 47].

4.4 Measures of station importance

To measure the importance of each station in a network, we take a topological approach. Centrality measures are a common heuristic used to rank node and link importance for adaptation and recovery prioritization (e.g., [4, 31, 38, 40, 49]). Conceptually, this uses a station's position as a proxy for its contribution to the integrity of an RTN. First, we measure centrality scores for each station in a network. Then, stations are sorted from highest to lowest score to develop a priority ranking. For adaptation, such rankings can be integrated with models of natural hazard exposure and used to support decisions for investments in hardening measures, such as flood-proofing and the installation of fail-safe mechanisms (e.g., [7, 12, 42]). For recovery, priority rankings can be used to triage damaged assets, informing repair crew scheduling protocols (e.g., [33, 49, 50]). Five metrics were selected for use as station-level measures of importance for adaptation and recovery prioritization: degree (DC), closeness (CC), and betweenness (BC) centrality, δ-efficiency (δE), and ridership-weighted betweenness centrality (RWBC).

Degree centrality is the count of neighboring stations adjacent to a given node. Consequently, degree is integer-valued. The vast majority of stations within the NEC ($n = 1322$, 79.7%) possess a degree of 2, reflecting one inbound and one outbound connection. The termini at the far ends of transit lines have a degree of 1 ($n = 114$, 6.87%), while interchanges and central hubs connecting multiple lines, or those serving as junctions at the convergence of lines, exhibit degrees greater than two ($n = 222$, 13.4%). This is expressed as $\mathrm{DC}(j) = \deg(j)$.

Betweenness centrality (Equation 5) measures the fraction of shortest paths between each pair of nodes in a graph that pass through node j. Consequently, structural 'bottlenecks' in the network will possess high betweenness; this makes BC a useful metric for identifying stations for hardening and recovery prioritization, as their

failure can significantly impede travel along high-traffic corridors.

$$\mathrm{BC}(j) = \sum_{i \neq j \neq k \in V} \frac{\sigma_{ik}(j)}{\sigma_{ik}} \tag{5}$$

Closeness centrality (Equation 6) is a measure of the inverse distance between a j and all other nodes $i \in E \setminus j$, normalized by node count. This makes closeness a useful metric for identifying stations that are central in terms of low travel cost to destinations throughout the NEC.

$$\mathrm{CC}(j) = \frac{N-1}{\sum_{i \neq j \in V} d(i,j)} \tag{6}$$

Following Saadat et al. [39], we define δ-efficiency (δE) as the weighted global network efficiency of a graph upon removal of j, normalized by the ideal efficiency prior to removal. This provides a measure of the impact that a disruption at j has on the overall travel cost throughout the network. Equation 7 defines δE in terms of unity minus the ratio of efficiency upon removing node j to the efficiency of the fully intact network, providing a normalized measure that maintains interpretive consistency with other metrics (higher scores indicate greater importance).

$$\delta E(j) = 1 - \frac{E_{\mathrm{glob}}\left(G \setminus j\right)}{E_{\mathrm{glob}}\left(G\right)} \tag{7}$$

Peripheral interchanges exhibited high ridership relative to nearby non-interchange stations. To test the hypothesis that controlling for ridership would better align local and global results, station-level ridership was incorporated into betweenness centrality. However, these patterns persisted when ridership weighting was factored in, supporting this study's broader conclusions.

Ridership-weighted betweenness centrality (RWBC, Equation 8) is defined following Ye et al. [51]. RWBC modifies BC by weighting the shortest path of each node pair proportional to φ_{ik}, the volume of passenger flow between end nodes. For each term to be summed, $\sigma_{ik}(j) \in \{0, 1\}$ is a boolean indicator equaling 1 if the shortest path between i and k passes through j, and is 0 otherwise. RWBC multiplies each $\sigma_{ik}(j)$ by flow φ_{ik}. This weights each path proportional to its passenger demand in order to better reflect ridership throughout the network. For S-L, RWBC considers only the ridership totals corresponding to a particular RTN, while S-G includes all NEC ridership during trip generation.

$$\mathrm{RWBC}(j) = \sum_{i \neq j \neq k \in V} \varphi_{ik} \frac{\sigma_{ik}(j)}{\sigma_{ik}} \tag{8}$$

4.5 Rank-shift analysis

Changes in station importance ranking between S-L and S-G (Figures 3-4) were calculated as follows. For a given importance metric $h(v)$ (DC, CC, BC, δE, RWBC) and a given system k with subgraph $S_k(V_k, E_k)$, $h(i)$ is evaluated for each station $i \in V_k$.

Values of $h(i)$ are sorted descending as set $R(S_k)$, with $R(S_k, i)$ giving the local ranking of station i. This is repeated globally with the same $h(i)$ and V_k within NEC graph $G(V, E)$. The subgraph $G[S_k]$ is then induced before scores are sorted to give global rankings $R(G_k)$. The distinction between S-L and S-G is that $R(G_k)$ is measured while connections and ridership between system k and the rest of the network $G \setminus S_k$ are still present, meaning S-G reflects the importance of each station to the entire NEC, while under S-L, $R(S_k)$ isolates S_k from other systems prior to measurement.

We define $R(S_k, i)$ at the local ranking of station i corresponding to its global ranking $R(G_k, i)$. This allows us to express $\delta R_{G \to S}(i) = R(G_k, i) - R(S_k, i)$, the global-to-local rank shift of i. For example, Figure 4**.a** shows South Station as the $R(G_k, i) = 1^{\text{st}}$ globally-ranked station in the MBTA Subway. Locally, South Station is ranked 9^{th} as $R(S_k, i) = 9$. This yields $\delta R_{G \to S}(i) = (1 - 9) = -8$, a global-to-local rank shift of eight. The same is done for global-to-local shifts as $\delta R_{S \to G}(j) = R(S_k, j) - R(G_k, j)$. Continuing the MBTA Subway example, Park Street is ranked $R(S_k, j) = 1^{\text{st}}$ locally, and $R(G_k, j) = 6^{\text{th}}$ globally. This yields $\delta R_{S \to G}(i) = (1 - 6) = -5$, a five-place drop. This is shown in greater detail in Figure 4: left columns show $R(S_k)$ and right columns show $R(G_k)$, with selections of k being the MBTA Subway and Commuter Rail and Amtrak, and $h(i) = \text{RWBC}(i)$.

The absolute value of rank shifts for a given system is a function of that system's station count, prohibiting direct comparison prior to normalization. For example, the observed maximum absolute rank shift in the NYC Subway is 416; the largest possible rank shift in a system is one less than the total station count, giving the NYC Subway a theoretical maximum of $|V_k| - 1 = 422$. In contrast, PATH possesses only $|V_k| = 13$ stations, with an observed maximum absolute shift of 10. To correct for this, prior to averaging, each rank shift is rescaled via dividing by $|V_k|$, where k is one of $K = 15$ rail systems. The formula for normalized average shift of rank m is shown in Equation 9, where i_m is the m^{th}-ranked station globally (if $\delta \bar{R}_{G \to S}$ or locally (if $\delta \bar{R}_{S \to G}$).

$$\delta \bar{R}_{X \to Y}(i_m) = \frac{1}{K} \sum_{k=1}^{K} \left(\frac{\delta R^k_{X \to Y}(i_m)}{|V_k|} \right) \tag{9}$$

4.6 Resilience quantification

System performance is measured as global network efficiency E_{glob} (Equation 10). Efficiency is calculated as the sum of inverse shortest paths between all node pairs, divided by the total pair count $N(N-1)$ to produce a normalized score.

$$E_{\text{glob}}(G) = \frac{1}{N(N-1)} \sum_{i \neq j \in V} \frac{1}{d_{ij}} \tag{10}$$

Instantaneous resilience $\rho_{\text{i}}(G(t))$ is measured as the efficiency of network G at time t normalized by the efficiency of the unperturbed network $G(t_0)$ (Equation 11). This is simply the fraction of performance relative to the expected level in the absence of

disruption.

$$\rho_{\mathrm{i}}(G(t)) = \frac{E_{\mathrm{glob}}[G(t)]}{E_{\mathrm{glob}}[G(t_0)]} \tag{11}$$

Total resilience during failure and recovery are denoted as ρ_{f} and ρ_{r}, respectively. The initiation of simulation time immediately prior to the first node removal is denoted t_0. The timestep immediately following the cessation of disruption and preceding the initiation of recovery, when performance is at a minimum, is denoted $t_{\text{f-r}}$, and the timestep upon restoration of performance to pre-disruption levels as t_{r}. ρ_{f} and ρ_{r} are then defined as the summation of all ρ_{i} during respective phases normalized as a fraction of baseline performance over the same duration (Equations 13, 12).

$$\rho_{\mathrm{f}}(G) = \frac{\sum_{t=t_0}^{t_{\text{f-r}}} \rho_{\mathrm{i}}(G(t))}{(t_{\mathrm{f}} - t_0)\rho_{\mathrm{i}}(G(t_0))} \tag{12}$$

$$\rho_{\mathrm{r}}(G) = \frac{\sum_{t=t_{\text{f-r}}}^{t_{\mathrm{r}}} \rho_{\mathrm{i}}(G(t))}{(t_{\mathrm{r}} - t_{\text{f-r}})\rho_{\mathrm{i}}(G(t_0))} \tag{13}$$

Total resilience for each system and changes in resilience between S-L and S-G are reported (Fig. 6). For failure, results are reported as $1 - \rho_f$. Targeting sequences that result in lower robustness values ρ_{f} are effective at degrading performance, implying that the corresponding strategy is effective at identifying critical stations for which protective measures should be prioritized. Consequently, larger values of $1-\rho_{\mathrm{f}}$ indicate greater efficacy. This maintains consistency in visual interpretation across failure and recovery results reported in Figure 6.

A small-magnitude slope indicates that R-L is more sensitive to choice of prioritization strategy relative to R-G. This is observed most consistently in systems positioned peripherally within the NEC, such as in Eastern New England and greater Washington, D.C. A large-magnitude slope indicates the opposite, with R-G exhibiting a greater sensitivity to strategy choice while R-L remains relatively consistent. A slope of $|m| \approx 1$ indicates proportionally approximate sensitivity of local and global resilience to strategy choice.

$$m_{L \to G} = \frac{\rho(G_G) - \rho(G_S)}{\rho(S_G) - \rho(S_S)} \tag{14}$$

Ethics and responsibility ChatGPT 5 Pro and Deep Research were used to assist in literature review, for minor code generation limited to visualization and data processing, and suggestion of manuscript structure. LLMs were not used in the article writing or editing process, nor for the analysis or interpretation of results.

5 Data availability

All data used in this study was sourced from publicly accessible repositories. See Supplementary Information for data sources. Rail transit network and ridership data is included in the GitHub repository listed under *Code availability*.

6 Code availability

Code used to produce the results of this study is available on GitHub: https://github.com/jack-watson/NEC_resilience/.

All analysis involved in this study was programmed in MATLAB, with some aspects of visualization and preprocessing of rail network data performed with ArcGIS Pro.

Acknowledgments. The authors would like to acknowledge Dr. Raviraj Dave, Danish Mansoor, and Aayushi Mishra for their generous contributions to the production of this research article.

==========

References

[1] Lauriat, G.: The northeast corridor – money is the "m" in megalopolis. American Journal of Transportation (752), 14 (2023)

[2] Xu, Z., Chopra, S.S.: Interconnectedness enhances network resilience of multimodal public transportation systems for Safe-to-Fail urban mobility. Nat. Commun. **14**(4291), 1–11 (2023) https://doi.org/10.1038/s41467-023-39999-w

[3] Pan, S., Yan, H., He, J., He, Z.: Vulnerability and resilience of transportation systems: A recent literature review. Physica A: Statistical Mechanics and its Applications **581**, 126235 (2021) https://doi.org/10.1016/j.physa.2021.126235

[4] Yadav, N., Chatterjee, S., Ganguly, A.R.: Resilience of Urban Transport Network-of-Networks under Intense Flood Hazards Exacerbated by Targeted Attacks. Sci. Rep. **10**(10350), 1–14 (2020) https://doi.org/10.1038/s41598-020-66049-y

[5] Sneider, J.: Hurricane sandy: Four years later, new york city transit is still fixing, fortifying the rail system. Progressive Railroading (2016). Rail News: Passenger Rail (November 2016). Accessed 2025-07-17

[6] Staff, N.Y.R.: Assessing the Damage From Hurricane Sandy. N.Y. Times (2012)

[7] Chan, R., Schofer, J.L.: Measuring Transportation System Resilience: Response of Rail Transit to Weather Disruptions. Nat. Hazard. Rev. **17**(1), 05015004 (2016) https://doi.org/10.1061/(ASCE)NH.1527-6996.0000200

[8] Ju, Y., Yuan, H., Li, Z., Gan, M., Chen, Y.: Multilayer structures and resilience evaluation for multimode regional rail transit system. IET Intel. Transport Syst. **16**(7), 843–859 (2022) https://doi.org/10.1049/itr2.12179

[9] Bi, W., Hackl, J., MacAskill, K.: Enhancing flood resilience of urban rail transit systems through recovery resource scheduling optimisation: A case study of London. Sustainable Cities and Society **128**, 106437 (2025) https://doi.org/10.1016/j.scs.2025.106437

[10] Bhatia, U., Kumar, D., Kodra, E., Ganguly, A.R.: Network Science Based Quantification of Resilience Demonstrated on the Indian Railways Network. PLoS One **10**(11), 0141890 (2015) https://doi.org/10.1371/journal.pone.0141890

[11] Chen, X., Ma, S., Chen, L., Yang, L.: Resilience measurement and analysis of intercity public transportation network. Transportation Research Part D: Transport and Environment **131**, 104202 (2024) https://doi.org/10.1016/j.trd.2024.104202

[12] Ippolito, N., Cats, O.: Multi-modal and multi-layer robustness analysis of the European rail and air networks. Sci. Rep. **14**(26950), 1–12 (2024) https://doi.org/10.1038/s41598-024-76264-6

[13] Yang, Z., Liu, X., Wang, J., Yan, X., Shen, R., Huo, Z.: Assessment on resilience of urban agglomeration transportation system considering passenger choice and load-capacity factor. Reliab. Eng. Syst. Saf. **253**, 110527 (2025) https://doi.org/10.1016/j.ress.2024.110527

[14] Northeast Corridor Commission: Northeast corridor commuter and intercity rail cost allocation policy. Technical report, Northeast Corridor Commission, Washington, DC (July 2025). Version 14.00 (file dated 2025-07-08). https://nec-commission.com/app/uploads/2018/04/2025-07-08_Cost-Allocation-Policy_v14.00_For-Publication-2.pdf

[15] Heddebaut, O.: Creating sustainable and efficient transport interchanges: Some findings of the city-hub project. Advancements in Civil Engineering amp; Technology **1**(5) (2018) https://doi.org/10.31031/acet.2018.01.000525

[16] Bohl, C.C.: Will Boston Ever Build the North-South Rail Link? Boston.com. Accessed 29 October 2025. https://www.boston.com/news/wickedpedia/2024/03/19/will-boston-ever-build-the-north-south-rail-link/

[17] Ivanov, I.T., Zimmermann, T., Heinrich, N.W.: Limits of disclosure regulation in the municipal bond market. Management Science **71**(10), 8452–8470 (2025) https://doi.org/10.1287/mnsc.2022.02289

[18] Marlowe, J.: Municipal bonds and infrastructure development—past, present, and future. A Policy Issue White Paper Prepared on behalf of the ICMA Governmental Affairs and Policy Committee (2015)

[19] Filatova, T., Taberna, A., Chatzivasileiadis, T., Cortés Arbués, I.: Private sector investments in climate change adaptation. Nature Climate Change (2025) https://doi.org/10.1038/s41558-025-02423-w

[20] Cornaggia, J., Cornaggia, K.J., Israelsen, R.D.: Credit ratings and the cost of municipal financing. The Review of Financial Studies **31**(6), 2038–2079 (2017) https://doi.org/10.1093/rfs/hhx094

[21] Gao, P., Lee, C., Murphy, D.: Municipal borrowing costs and state policies for distressed municipalities. Journal of Financial Economics **132**(2), 404–426 (2019)

[22] Hernandez, S., Monzon, A.: Key factors for defining an efficient urban transport interchange: Users' perceptions. Cities **50**, 158–167 (2016) https://doi.org/10.1016/j.cities.2015.09.009

[23] Yap, M., Wong, H., Cats, O.: Passenger valuation of interchanges in urban public transport. Journal of Public Transportation **26**, 100089 (2024) https://doi.org/10.1016/j.jpubtr.2024.100089

[24] Vanderwaart, C.C.E.: Planning transit networks with origin, destination, and interchange inference. PhD thesis, Massachusetts Institute of Technology (2016)

[25] Martello, M.V., Whittle, A.J., Lyons-Galante, H.R.: Depth-damage curves for rail rapid transit infrastructure. Journal of Flood Risk Management **16**(1), 12856 (2023)

[26] Bi, W., Linkov, I., MacAskill, K.: Supporting urban sustainability through resilient rail transit systems. Cities **167**, 106373 (2025) https://doi.org/10.1016/j.cities.2025.106373

[27] Sun, X., Lin, S., Feng, D., Zhang, Q.: Post-disaster repair optimization method for traction power supply system of electrified railways based on train operation loss. Reliab. Eng. Syst. Saf. **250**, 110301 (2024) https://doi.org/10.1016/j.ress.2024.110301

[28] Ilalokhoin, O., Pant, R., Hall, J.W.: A model and methodology for resilience assessment of interdependent rail networks – Case study of Great Britain's rail network. Reliab. Eng. Syst. Saf. **229**, 108895 (2023) https://doi.org/10.1016/j.ress.2022.108895

[29] Jiao, L., Li, D., Zhang, Y., Zhu, Y., Huo, X., Wu, Y.: Identification of the key influencing factors of urban rail transit station resilience against disasters caused by rainstorms. Land **10**(12), 1298 (2021) https://doi.org/10.3390/land10121298

[30] Martello, M.V., Whittle, A.J.: Estimating coastal flood damage costs to transit infrastructure under future sea level rise. Communications Earth amp; Environment **4**(1) (2023) https://doi.org/10.1038/s43247-023-00804-7

[31] Zheng, M., Zuo, H., Zhou, Z., Bai, Y.: Recovery Strategies for Urban Rail Transit Network Based on Comprehensive Resilience. Sustainability **15**(20), 15018 (2023) https://doi.org/10.3390/su152015018

[32] Trakas, D.N., Hatziargyriou, N.D.: Strengthening transmission system resilience against extreme weather events by undergrounding selected lines. IEEE Transactions on Power Systems **37**(4), 2808–2820 (2022) https://doi.org/10.1109/tpwrs.

2021.3128020

[33] Massobrio, R., Cats, O.: Topological assessment of recoverability in public transport networks. Commun. Phys. **7**(108), 1–9 (2024) https://doi.org/10.1038/s42005-024-01596-8

[34] Zhang, Y., Ayyub, B.M., Saadat, Y., Zhang, D., Huang, H.: A double-weighted vulnerability assessment model for metrorail transit networks and its application in Shanghai metro. Int. J. Crit. Infrastruct. Prot. **29**, 100358 (2020) https://doi.org/10.1016/j.ijcip.2020.100358

[35] Xu, C., Xu, X.: A two-stage resilience promotion approach for urban rail transit networks based on topology enhancement and recovery optimization. Physica A **635**, 129496 (2024) https://doi.org/10.1016/j.physa.2024.129496

[36] Chen, J., Liu, X., Hu, X., Du, B., Yin, Y.: Resilience assessment of an urban rail transit network under natural disasters. Transportation Research Part D: Transport and Environment **139**, 104587 (2025) https://doi.org/10.1016/j.trd.2024.104587

[37] Wu, F., Schonfeld, P.M., Ayyub, B., Kim, M.: Topological Approach for Optimizing Railroad Freight Network Restoration after Disruptions. Transp. Res. Rec. **2676**(12), 750–759 (2022) https://doi.org/10.1177/03611981221097397

[38] Meng, Y., Tian, X., Li, Z., Zhou, W., Zhou, Z., Zhong, M.: Exploring node importance evolution of weighted complex networks in urban rail transit. Physica A **558**, 124925 (2020) https://doi.org/10.1016/j.physa.2020.124925

[39] Saadat, Y., Ayyub, B.M., Zhang, Y., Zhang, D., Huang, H.: Resilience-Based Strategies for Topology Enhancement and Recovery of Metrorail Transit Networks. ASCE-ASME Journal of Risk and Uncertainty in Engineering Systems, Part A: Civil Engineering **6**(2), 04020017 (2020) https://doi.org/10.1061/AJRUA6.0001057

[40] Song, J., Ding, J., Gui, X., Zhu, Y.: Assessment and solutions for vulnerability of urban rail transit network based on complex network theory: A case study of Chongqing. Heliyon **10**(5), 27237 (2024) https://doi.org/10.1016/j.heliyon.2024.e27237

[41] Ma, Z., Yang, X., Wu, J., Chen, A., Wei, Y., Gao, Z.: Measuring the resilience of an urban rail transit network: A multi-dimensional evaluation model. Transport Policy **129**, 38–50 (2022) https://doi.org/10.1016/j.tranpol.2022.10.003

[42] Wang, Y., Zhao, O., Zhang, L.: Modeling urban rail transit system resilience under natural disasters: A two-layer network framework based on link flow. Reliab. Eng. Syst. Saf. **241**, 109619 (2024) https://doi.org/10.1016/j.ress.2023.109619

[43] Wang, X., Koç, Y., Derrible, S., Ahmad, S.N., Kooij, R.E.: Quantifying the robustness of metro networks. arXiv (2015) https://doi.org/10.48550/arXiv.1505.06664 1505.06664

[44] Zhang, J., Wang, S., Wang, X.: Comparison analysis on vulnerability of metro networks based on complex network. Physica A **496**, 72–78 (2018) https://doi.org/10.1016/j.physa.2017.12.094

[45] Cubukcu, K.M.: Using circuity as a network efficiency measure: the example of Paris. Spat. Inf. Res. **29**(2), 163–172 (2021) https://doi.org/10.1007/s41324-020-00342-w

[46] Goh, S., Lee, K., Park, J.S., Choi, M.Y.: Modification of the gravity model and application to the metropolitan seoul subway system. Physical Review E **86**(2) (2012) https://doi.org/10.1103/physreve.86.026102

[47] Wang, Z., Chen, Y.: Exploring spatial patterns of interurban passenger flows using dual gravity models. Entropy **24**(12), 1792 (2022) https://doi.org/10.3390/e24121792

[48] Chen, Y.: The distance-decay function of geographical gravity model: Power law or exponential law? Chaos, Solitons amp; Fractals **77**, 174–189 (2015) https://doi.org/10.1016/j.chaos.2015.05.022

[49] Bhatia, U., Sela, L., Ganguly, A.R.: Hybrid Method of Recovery: Combining Topology and Optimization for Transportation Systems. J. Infrastruct. Syst. **26**(3), 04020024 (2020) https://doi.org/10.1061/(ASCE)IS.1943-555X.0000566

[50] Pan, X., Wang, H.: Resilience of and recovery strategies for weighted networks. PLoS One **13**(9), 0203894 (2018) https://doi.org/10.1371/journal.pone.0203894

[51] Ye, P., Wu, B., Fan, W.: Modified betweenness-based measure for prediction of traffic flow on urban roads. Transportation Research Record: Journal of the Transportation Research Board **2563**(1), 144–150 (2016) https://doi.org/10.3141/2563-19

Supplementary Files

This is a list of supplementary files associated with this preprint. Click to download.

- NECsupplementsubmissionv0111Nov2025.pdf